AIAA-2000-2562

REDUCED-BASIS MODEL FOR ACTIVE SEPARATION CONTROL IN A PLANAR DIFFUSER FLOW

Brianno D. Coller*, Bernd R. Noack†‡, Satish Narayanan‡,
Andrzej Banaszuk‡, Alexander I. Khibnik‡

Abstract

The diffuser flow is investigated experimentally and described theoretically in an ongoing effort toward flow control guided by physics-based, reduced-order models. The diffuser consists of a straight channel section and an asymmetric diverging section in which the upper wall is aligned with the flow and the lower wall is inclined at 23°. The Reynolds number based on maximum inlet velocity and channel height is $Re = 70000$ and the incoming flow has a fully developed turbulent boundary layer. The diffuser pressure recovery was found to be enhanced in the experimental studies by excitation of coherent structures with a time-periodic actuation (provided acoustically through a slot at the diffuser inlet). The experimentally observed flow response to actuation involving the formation of coherent vortical motion is qualitatively well described by a two-dimensional vortex-based model. In particular, the pronounced vortex formation at an "optimal" actuation frequency corresponding to enhanced pressure recovery is observed. The pressure recovery mechanisms are discussed using a control volume model applied to experimental and theoretical data.

1 Introduction

Separation phenomena are relevant to many industrial and military applications. Examples are external flows e.g. airfoils at large angle of attack, and internal flows such as aggressively expanding diffusers. Typically, separation results in performance deterioration of flow devices, hence the active pursuit of separation control.

Various means for preventing or delaying the onset of separation have been proposed, including passive methods such as vortex generators, and active methods such as steady blowing and suction techniques, mechanical rotor type actuators and synthetic jets [1]. In some studies, the use of unsteady actuation for mitigating/delaying separation has been explored with the aim of reducing actuation penalties when compared to steady active methods. Mechanical actuators at the surface close to the separation region have been studied in low speed flows [2][3]. Pulsed jets arranged on the surface of the flow past a two-dimensional airfoil section were also used to delay separation [4]. The success of such control has been attributed to to the excitation of 'favorable' large-scale organized motion in the flow. In numerical simulations [5], the effectiveness of unsteady control in changing the flow structures was demonstrated at high Mach number M and low Reynolds number Re flow with laminar boundary layers. Separation control of incompressible, turbulent boundary layers in diffusers was numerically studied by Driller [6]. The adverse effect of separation at an airfoil with high angle of attack was successfully reduced with periodic blowing by Wygnanski et al. [7][8]. A phenomenological explanation of the control effect was proposed, but a dynamical model of the observed flow phenomena has not emerged.

Optimization of the control parameters and recommendation of new unsteady separation control strategies rely heavily on experimentation in laboratory scale models with the hope that favorable results will be obtained in full-scale devices. Numerical simulations of separation control techniques are expensive for high-Reynolds number flows, hence unsuitable for exploratory studies. The optimization of forcing parameters requires reduced-order models (ROMs), capturing the dominant/relevant coher-

*Department of Mechanical Engineering, University of Illinois at Chicago, Chicago, IL 60607-7022

†New address: Hermann-Föttinger-Institut für Strömungsmechanik, Technische Universität Berlin, Straße des 17. Juni 135, D-10623 Berlin, Germany

‡United Technologies Research Center, 411 Silver Lane MS 129-15, East Hartford, CT 06108

ent structure dynamics, the actuation effect and the associated performance achievement. There exists some recent attempts to use reduced-order models for separation control based on vortex models [9][10].

The aim of the present study is to evolve toward model-based control of coherent structures, allowing substantially lowered actuation requirements. The goals are (1) to identify the key physical phenomena responsible for pressure recovery, (2) to identify effective means/parameters for controlling these phenomena and associated dynamics, (3) to develop reduced-order models linking actuation with performance, and (4) to attempt to assess the fundamental limits of (achievable) performance. We chose a planar diffuser flow as a testbed for such model-based separation control.

The manuscript is organized as follows. In §2, 3, and 4, we describe the experimental setup, a vortex-based model for the flow evolution and a control-volume model for the pressure recovery analysis, respectively. In §5, corresponding experimental and numerical results are presented. These results are discussed in §6. Finally (in §7), a summary of the study and an outlook for the future direction is presented.

2 Experimental Setup

The experiments were performed in a two-dimensional air facility at UTRC. A facility schematic, displaying the velocity probe and static pressure tap locations, is shown in Fig. 1. The flow was operated in the range $70000 < Re_h < 140000$, with incoming fully developed turbulent boundary layers; H (=5.08 cm) is the inlet diffuser height. The corresponding incoming flow speeds were in the range of $20\,m/s < U < 40\,m/s$. The length of the expanding section is 4 channel heights. The two expanding sides of the inlet consist of flexible plexiglas pieces for a smooth transition to the diffusing section (see Fig. 1). An asymmetric diffuser configuration was studied with the upper wall in streamwise direction and the lower wall of the diffuser being moved to vary the expansion angle.

A single hot-film probe (model TSI 1210-20) was used to measure unsteady velocity signals ($u(t)$ in Fig. 1). Static pressure taps mounted on the parallel side walls were connected to a Cetra pressure transducer via short tubes for mean as well as unsteady (up to $100\,Hz$) pressure reocovery measurements. The performance of the diffuser is described by the pressure recovery coefficient $C_p = \Delta p/\frac{1}{2}\rho U^2$,

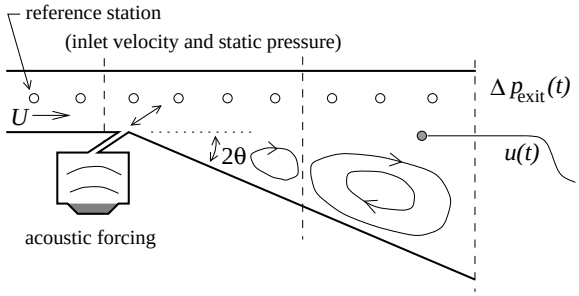

Figure 1: *Experimental facility schematic; the dashed lines indicate the streamwise locations at which mean and fluctuation profiles of the velocity were measured (reported later).*

the static pressure difference Δp between the values of a downstream pressure tab and the reference tap normalized with the dynamic inlet pressure $\frac{1}{2}\rho U^2$. Here, U denotes the inlet core velocity. A D-space system was used for data acquisition and to generate control signals for excitation. Smoke generated by heating oil was used to visualize the flow patterns under unforced and forced flow conditions. A $2\,cm$ thick Nd:Yag laser sheet (pulsed at $10\,Hz$) was used to illuminate the smoke in a vertical plane on the spanwise centerline of the diffuser. Long and short exposure visualization images were recorded on a VCR. Acoustic forcing was used for excitation. The excitation system comprises a $24\,cm \times 24\,cm \times 9\,cm$ box with a wall-mounted 8" JBL speaker and a $20cm$ long and $0.32\,cm$ wide slot providing effective excitation in the range $20\,Hz < f < 100\,Hz$. The slot exit was matched to an $18\,cm$ long and $0.32\,cm$ wide channel which transitions to an angled slot at the beginning of the expansion (see Fig. 1).

3 Vortex Model

We seek a moderate dimensional model that captures the essential dynamic features of the flow separation, roll up, and vortex pairing processes responsible for diffuser pressure recovery characteristics. Here, we represent the vorticity field by N point vortices, with individual circulations Γ_j and positions $\boldsymbol{z}_j$. According to two-dimensional vorticity formulation of the Navier-Stokes equation, the vorticity is simply carried with the fluid at the local velocity, and it diffuses at a rate proportional to the inverse of the Reynolds number. In previous numerical shear layer studies (*e.g.* Ghoniem and Ng

[11]), researchers find that the diffusive component of the vortex dynamics have little effect on the intrinsic roll-up and pairing dynamics. Therefore, we set $Re = \infty$ and ignore diffusion. Under these conditions, the evolution equations become ODEs:

$$\dot{\boldsymbol{z}}_j = \boldsymbol{u}(\boldsymbol{z}_j, t), \quad j \in 1, 2, 3, \ldots, N. \tag{1}$$

Here, the local velocity $\boldsymbol{u}(\boldsymbol{z}_j, t)$ depends on vorticity distribution, free-stream, and actuator:

$$\boldsymbol{u}(\boldsymbol{z}_j, t) = \sum_{k=1, \neq j}^{N} K(\boldsymbol{z}_j, \boldsymbol{z}_k)\Gamma_k \tag{2}$$

$$+\mathbf{u}_0(\boldsymbol{z}_j) + \mathbf{u}_a(\boldsymbol{z}_j, t). \tag{3}$$

K denotes the kernel the Biot-Savart law for point vortices, $\mathbf{u}_0$ the steady potential free-stream, and $\mathbf{u}_a$ the unsteady potential source actuator.

For the inviscid flow, the appropriate boundary condition is the non-penetration condition $\boldsymbol{u} \cdot \hat{\boldsymbol{n}} = 0$, where $\hat{\boldsymbol{n}}$ is a vector perpendicular to the boundary. This is facilitated with the aid of conformal mapping. The *physical domain* is parameterized by the complex coordinate $z = x + iy$. To this we associate the *transformed domain*, $\mathrm{Im}\{\zeta\} \geq 0$. Both are depicted in Figure 2. We represent the analytic transformation and inverse between the physical and transformed domains compactly by $\zeta(z)$ and $z(\zeta)$. According to the Schwarz-Christoffel theorem [12], the derivative of the transformation may be expressed as a simple monomial. Specifically, for the transformation shown in Figure 2 which we shall use throughout this paper, the derivative is given by

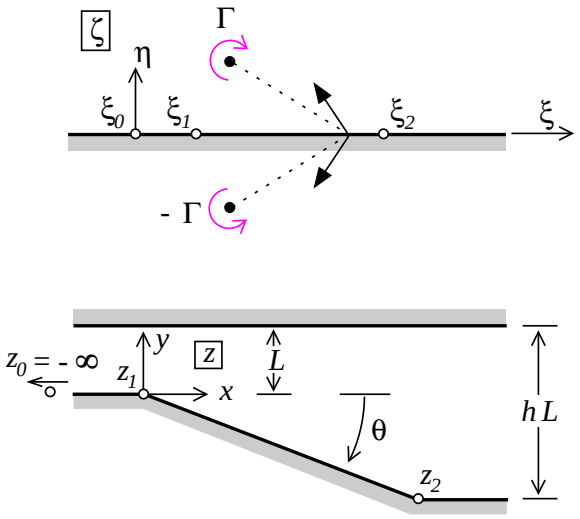

Figure 2: *Transformed and physical domains for the diffuser problem.*

$$\frac{dz}{d\zeta} = \frac{h(\zeta - \xi_1)^{\vartheta}}{(\zeta - \xi_0)(\zeta - \xi_2)^{\vartheta}}, \tag{4}$$

where ϑ is related to the diffuser angle θ via $\vartheta = \theta/\pi$. For our specific problem, $\xi_0 = 0$, $\xi_1 = 1$, and $\xi_2 = h^{1/\vartheta}$. The pre-vertices ξ_0, ξ_1, and ξ_2 map to z_0, z_1, and z_2, respectively.

Given a complex velocity potential $\Phi_\zeta(\zeta)$ in the transformed domain, we derive the corresponding potential in the physical plane as $\Phi_z(z) := \Phi_\zeta(\zeta(z))$. The velocity at a point $\hat{z}$ in the physical domain is thus calculated by

$$\bar{v}(\hat{z}) = \left.\frac{d\Phi_z}{dz}\right|_{z=\hat{z}} = \left.\frac{d\Phi_\zeta}{d\zeta}\right|_{\hat{\zeta}} \left.\frac{d\zeta}{dz}\right|_{\hat{z}}, \tag{5}$$

where $\hat{\zeta} = \zeta(\hat{z})$.

Here, we shall place all flow elements in the transformed domain, then size and evolve them according to (2) in the physical plane. To begin, we place a source at the $\zeta = \xi_0 = 0$ of strength $2\pi^2$ to represent the potential free-stream $\mathbf{u}_0$ in (2). With this choice, the average flow speed U well upstream of the expansion in the physical domain is the length L per unit time. For each vortex in the transformed domain, $\mathrm{Im}\{\zeta\} > 0$, we place an image vortex of opposite circulation in the half plane $\mathrm{Im}\{\zeta\} < 0$ in order to ensure that the non-penetration boundary condition is satisfied at $\mathrm{Im}\{\zeta\} = 0$. Since the transformation is conformal except at the two finite vertices, the non-penetration condition is preserved in the physical domain.

After considerable work, one obtains equations of motions for the vortices within the transformed domain. If we let ζ_j denote the position of the j^{th} vortex, then

$$\frac{d\zeta_j}{dt} = \frac{1}{|dz/d\zeta|^2}\left[\frac{d\tilde{\Phi}_j}{d\zeta} - \frac{i\Gamma_j}{4\pi(dz/d\zeta)}\frac{d^2z}{d\zeta^2}\right]. \tag{6}$$

Here,

$$\tilde{\Phi}_j = \Phi_\zeta(\zeta) - \frac{i\Gamma_j}{2\pi}\log(\zeta - \zeta_j) \tag{7}$$

is the velocity potential in the transformed domain due to free-stream, actuation and all vortices except the j^{th} one. The second term within the brackets in (6) comes from a limiting process in the transformation, which incorporates the turning of the flow

around sharp corners. The factor outside the square brackets on the right hand side of (6) accounts for scaling in the transformation. Since we do not have an explicit formula for the transformation in terms of elementary functions, we have formulated the entire problem in the transformed domain; all derivatives are with respect to transform variables.

Vortex elements are introduced into the flow in order to satisfy an unsteady Kutta condition at the convex corner z_1. New vortex strengths and locations are chosen to make the velocity at $\zeta = \xi_1$ in the transformed domain, and hence make the velocity in the physical domain at z_1 finite. We satisfy the Kutta condition by employing a variation of an approach developed by [13].

A new vortex is introduced into the model at each time step. The separating shear-layer was found be well resolved with fifty vortices being added each convective unit of time. Care must be taken so that the problem size does not grow without bound. Sufficiently far downstream of the expanding section of the physical domain, we begin merging nearby vortices. At about forty characteristic lengths downstream of the expanding section, we remove the vortices completely. The merging strategy is successfully employed by Shiels [14] in very high resolution simulation of flow past a circular cylinder. The strategy in our closed flow is complicated by the fact that strong vortices which have gone through several mergings occasionally get caught in a recirculation zone which draw them upstream, affecting the vortex dynamics in this sensitive regions in non-physical ways. To prevent this, we also incorporate a vortex splitting scheme for vortices traveling against the mean flow.

Finally, to mimic the effect of the actuator in the experiment, i.e. $\mathbf{u}_a$ in (2) we place a variable strength source on the real axis just downstream of $\zeta = \xi_1$. Below, we report results for which the strength of this "source" is varied sinusoidally with zero mean. The location of the source and its amplitude are chosen carefully so that momentum flux is comparable to that in the experiment, as well as the velocity at the pre-vertex ξ_1 where the rate of circulation production is determined.

4 Control–Volume Model

In this section, the pressure recovery coefficient associated with two streamwise locations is related to the corresponding velocity and fluctuation profiles. The resulting control-volume model provides insight in the upper bound for the pressure recovery and how the sub-optimal diffuser performance is linked to mean flow and fluctuations. The predictions of the control-volume model are compared with experimental data (§5.1) and employed in the vortex model (§3, 5.2).

The control-volume model is developed for incompressible flow since the Mach number in the diffuser experiment is small (< 0.1) and since the vortex model also assumes a divergence-free velocity field. The model is based on the boundary-layer approximation, i.e. the pressure field is assumed to be dependent on the streamwise coordinate and the velocity field is assumed to be locally approximated by parallel flow. The boundary-layer approximation at the considered diffuser geometry, i.e. 23° inclination of the lower wall, stretches the typical range of applicability and is discussed after the derivation. A second assumption is negligible internal dissipation. This ideal-flow assumption is a commonly used approximation if internal flow is dominated by a potential core region [15]. The pressure drop due to internal friction is shown to be negligible under more general conditions [16].

Let x,y,z be the coordinates of a Cartesian coordinate system where the origin lies in the center of the plane separating the channel and the diverging section of the diffuser (see Fig. 3). The x-axis is aligned with the flow and the y-axis is normal to the upper and lower wall of the channel section, and the z-axis corresponds to the spanwise direction. Let Ω denote a domain in the diffuser associated with the x-interval $x_1 < x < x_2$. In the sequel, the subscripts 1,2 refer to quantities in the planes $x = x_1$ and $x = x_2$, respectively. The mass-averaged velocity and diffuser height at planes $x = x_n$ are denoted by U_n and H_n, respectively. Typically, $x = x_1$ and $x = x_2$ represent the diffuser inlet and exit planes across which the pressure-recovery coefficients are determined (§2). Let u,v,w denote the velocity components in x-, y-, and z-direction, respectively, $\mathbf{u} = (u, v, w)$ the velocity vector, p the pressure, ρ the density and ν the kinematic viscosity of the fluid.

The boundary-layer approximation is employed in the equation of continuity and the inviscid energy balance for the diffuser section $x_1 < x < x_2$. A straight-forward calculation (see [16]) yields the pressure-recovery coefficient C_p in terms of the ve-

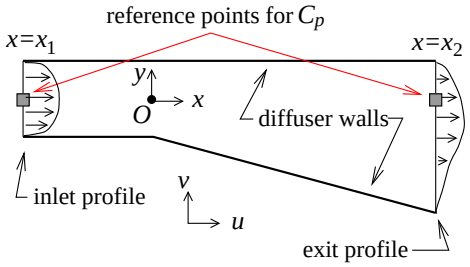

Figure 3: *Diffuser geometry and coordinate system*

locity and fluctuation profiles,

$$C_p = \frac{p_2 - p_1}{\frac{1}{2}\rho U_1^2} = C_p^0 + C_p^1; \qquad (8)$$

$$C_p^0 = \alpha_1^0 - \left[\frac{H_1}{H_2}\right]^2 \alpha_2^0;$$

$$C_p^1 = \alpha_1^1 - \left[\frac{H_1}{H_2}\right]^2 \alpha_2^1,$$

where

$$\alpha_n^0 = \frac{1}{h_n}\int dy\, \overline{u}^3/U_n^3, \quad \text{for} \quad n = 1, 2;$$

$$\alpha_n^1 = \frac{3}{h_n}\int dy\, \overline{u}\,\overline{(u')^2}/U_n^3 \quad \text{for} \quad n = 1, 2.$$

The coefficients α_n^0 characterize time-averaged profiles. The value is unity for uniform flow $u = U_n$ and larger for any non-constant profile. The value of the coefficient thus quantifies the deviation from uniform flow. The coefficients α_n^1 vanishes for steady flow and thus quantify the contribution of unsteadiness to the pressure recovery. Present control-volume models [15] neglect the effect of unsteadiness, i.e. C_p^1. The pressure-recovery coefficient of potential flow $C_p^{pot} = 1 - [H_1/H_2]^2$ (see, e.g., [15]), can be considered as the upper limit for diffuser flow.

The control volume model can easily be generalized for non-parallel flow assuming constant pressure across $x = x_n$. The steady and unsteady contribution of the v-component can be shown to be of order $O(v^2/U^2)$, assuming mean and fluctuation of the same order of magnitude. The w-component is expected to be noticeably smaller than the u- and v-component since it is not supported by a mean-flow production mechanism. The mean component of w can be expected to vanish or be small in a nominally planar diffuser. In the present diagnostic study, errors of the order of 10% are considered acceptable and the mean-flow contribution can thus be neglected even for moderate diffuser wall inclinations of $\sim 20°$. However, the fluctuation contribution of the v-component may be comparable to the one of the u-component. In this sense, C_p^1 can be considered an indicator of the effect of unsteadiness. In §5.3, the contribution of the fluctuation to the pressure-recovery coefficient is shown to be small. This justifies aposteriori the parallel-flow assumption.

5 Results

In this section, the experimental and theoretical results for the natural and periodically forced diffuser flow are described. In §5.1, the experimentally obtained velocity dynamics and pressure recovery data are outlined. In §5.2, corresponding simulations of the vortex model are discussed. Finally §5.3, the diffuser performance is analyzed using the control-volume model.

5.1 Experimental results for dynamic separation control

The goal of the experimental studies was to explore the sensivity of the large-scale coherent structure dynamics on actuation and how the coherent fluid motion effects the diffuser performance, i.e. pressure recovery. Thus, opportunities for efficient active separation control via coherent structures were explored and the key physics phenomena for reduced-order models were identified.

The flow field of the asymmetric diffuser configuration, with a diffuser angle of $2\theta \approx 23°$, is visualized using smoke. Fig. 4 displays transitory stall with large-scale separation, reverse flow regions close to the diffuser inlet (see tuffs on lower wall), and separated flow structures in the free-stream.

In open-loop forcing experiments, localized acoustic actuators at the diffuser inlet affect the separation dynamics. These diagnostic open-loop experiments enable exploration of the spatio-temporal behaviour of the flow structure underlying separation. The experiments also allow for correlating flow structures with the pressure recovery coefficient C_p.

Detailed experiments were performed at a few speeds and a few angles associated which transitory/steady stall. The forcing levels used were relatively low and were fixed for the results reported here. The corresponding non-dimensional momentum coefficient values are 0.2%. The procedure for

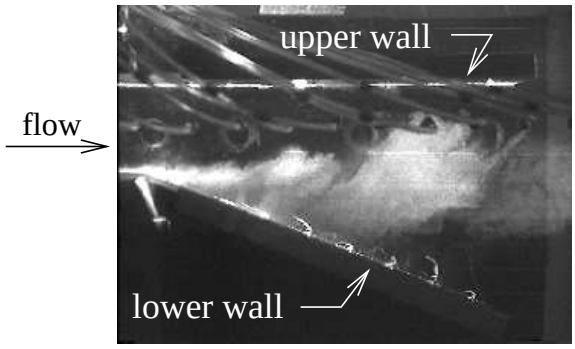

Figure 4: *Instantaneous smoke visualization snapshot of the natural flow displaying large-scale transitory stall in the diffuser at* $2\theta \approx 23^\circ$ *and inlet velocity* $U_1 = 20\,m/s$.

evaluating this measure of input control energy from velocity measurements at the excitation slot exit is the same as that used in an separate study of a planar diffuser (see [17]).

The forcing experiments reported here are for a diffuser angle of approximately 23°. Figure 5 displays the magnitude of the frequency response for acoustic forcing in the range $10\,Hz < f < 200\,Hz$, computed between the forcing signal and the mean pressure recovery coefficient C_p recorded near the diffuser exit (referenced to the upstream static pressure measurement) for three different maximum inlet flow speeds $U_1 \approx 20, 30, 40\,m/s$. The explored frequency range for the low-speed flow ($20\,m/s$) corresponds to a Strouhal number range of $0.025 < St_H = Hf/U_1 < 0.50$ based on channel height and inlet velocity. If not stated otherwise, all experimental forced flows results are based on inlet velocity $U_1 = 20\,m/s$ and actuation frequency $f = 30\,Hz$ ($St_H = 0.08$).

Sufficiently long averages (more than 100 ensemble averages) were used to obtain statistically converged frequency responses. Note the enhanced response of the unsteady pressure dynamics to forcing in the broadband frequency range surrounding the non-dimensional frequency range of $0.1 < St_H < 0.2$; Note that the C_p enhancements become less as the speed increases, presumably because the non-dimensional forcing amplitude (relative to the free-stream speed) decreases for a fixed input forcing amplitude (maintained constant for all the cases). Furthermore, note that the peak magnitude of the velocity amplitude provided by the actuator is a function of the forcing frequency alone, not the free-stream flow speed. Thus, the separated flow dynamics dictate the choice of preferred frequency bands for C_p enhancement.

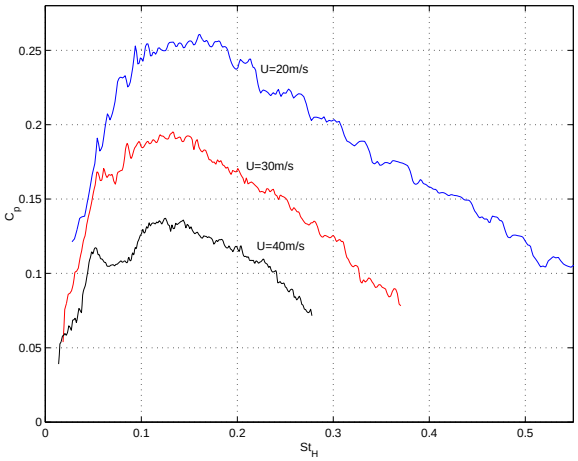

Figure 5: *Magnitudes of frequency responses for the diffuser mean pressure recovery coefficient* C_p *at three different inlet velocities* $U_1 = 20\,m/s$, $30\,m/s$, *and* $40\,m/s$. *The Strouhal frequency has been non-dimensionalized with the diffuser inlet channel height and the inlet core speed. The diffuser angle is* 23°.

Smoke flow visualization of the uncontrolled and controlled diffuser flows were performed to see the coherent structures. Figure 6 displays instantaneous snapshots of the unforced and a forced flow, displaying large-scale coherent structures in all the cases. The forcing frequency was chosen to be $f = 30Hz$ ($St_H = Hf/U_1 = 0.08$) which lies in a frequency band for which the C_p enhancement was maximum. Notice that smoke traces can be seen to be drawn to the lower wall in the forced flow indicating effective transport of high momentum fluid in the core region toward the lower wall. It is believed that the modified coherent structures in the forced flow are more effective in enhancing momentum exchange between the free-stream and the low-momentum, near-wall flow.

This time-averaged characteristics of the forced flow are visualized by long exposure recording of the smoke visualization images. The exposure time is about 30 seconds corresponding to about 12,000

convective time units. In Fig. 6, the structures of the unforced flow (c) are farther away from the lower diffuser wall than for forced flow. The forced flow with actuation Strouhal frequency of $St_H = 0.08$ (see Fig. 6(d)) displays an averaged flow field picture with the smoke-filled flow close to the lower wall for an extended streamwise extent up to the diffuser exit. Thus, the long-exposure visualization corroborate our conclusion that the large-scale coherent structures in the forced flow appear to be more effective for the transversal momentum transfer than natural flow.

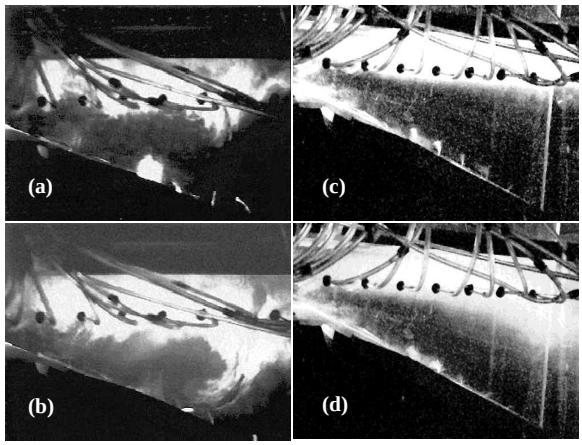

Figure 6: *Instantaneous snapshots of smoke visualization for the unforced (a) and forced flow (b), and corresponding long-time integrated visualization images for the unforced (c) and forced flow (d). The flow is from right to left with inlet velocity* $U_1 = 20\ m/s$. *The forcing frequency is* $f = 30\ Hz$, *i.e.* $St_H = 0.08$.

Time-averaged measurements of the mean velocity profile and fluctuation levels at the diffuser exit were made (see Fig. 7) to elucidate the effectiveness of the forced coherent structures in re-directing higher momentum flow toward the wall. Profiles were measured at three streamwise locations indicated in Fig. 1. These locations are $x/H \approx 0, 2.25, 4$. The profiles are displayed in Fig. 7 for the beginning of the diverging section (Fig. 7(a,b)), the midsection (Fig. 7(c,d)) and the expansion exit (Fig. 7(e,f)), respectively. The inlet flow was found the have shape factors characteristic for channel flow with fully developed turbulent boundary layers on both walls. The results downstream display deflection of the flow towards the lower wall as a result of forcing. A particularly effective deflection was evidenced at a forcing frequency associated with the largest C_p enhancement.

In summary, the above experiments aimed at understanding the unsteady characteristics of a separated flow in nominally planar diffuser under unforced and forced conditions revealed underlying organized spatiotemporal dynamics, and the dependence of average performance characteristics such as mean pressure recovery on the (organized) coherent structure dynamics. The experimental studies have resulted in: (i) a dynamical description of flow separation in the diffuser; (ii) identification of dynamic signatures associated with separation (viz. the critical spatial and temporal scales); and (iii) description and interpretation of the flow response (for dynamic as well as averaged characteristics) to unsteady forcing. In the following section we present a reduced-order model which captures the dynamics of these large-scale vortical motions, permitting control analysis.

5.2 Vortex model results for performance prediction

Experiments have indicated that control of transitory stall is associated with formation of shear-layer structures, which have been well described with vortex-based models in the literature. In this section, we simulate the evolution of the vortices using the vortex model discussed in §3 to gain insight into the dynamics and formation of the coherent flow structures. Care is taken to match geometry and actuation parameters of the experiment.

In Figure 8, we show profiles of the time averaged horizontal component of velocity computed for unforced flow and for open-loop forcing at Strouhal number 0.15, a dimensionless frequency roughly at the peak of the experimental pressure recovery curve in Figure 5. Before comparing these to the experimental profiles in Figure 7, we note that the hot-wire measurements used to collect the data for the experiment did not discern direction of the flow. Thus the mean back flow apparent in the computational profiles would appear as a positive speed as shown in the experimental data, if measured by the same hot wire. The backward-blown tufts along the bottom wall in Figure 4 and lack of smoke in the bottom portion of the long time exposures in Figures 6c,d indicate a potentially substantial recirculation region in a time-averaged sense. Time traces of the computational velocity signal are highly unsteady and

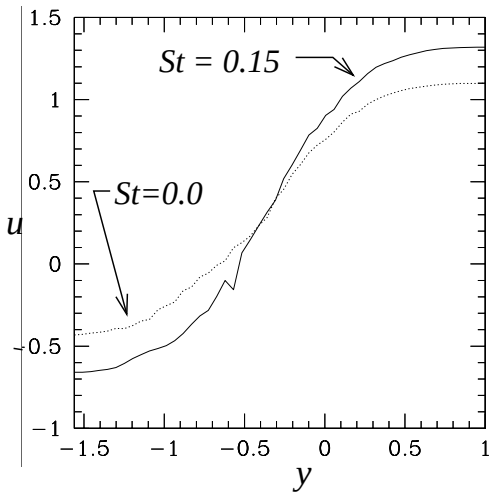

Figure 8: *Profile of horizontal component of velocity downstream of expansion in forced and unforced conditions predicted by the vortex model*

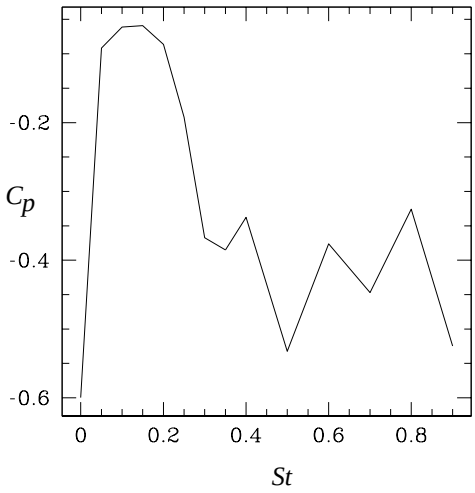

Figure 9: *Diffuser pressure recovery vs. Strouhal number predicted by vortex model.*

broad-band, indicating a transitory stall behavior as in the experiment.

Also like the experiment, the open-loop forcing tends to direct fluid momentum toward the bottom expanding wall on average, making the profile more full. The analysis in Section 4 indicates that more uniform exit profiles lead to improved pressure recovery. Employing the performance measures developed previously, we present in Figure 9 a plot of pressure recovery versus forcing frequency using velocity profile data from simulations. Quantitatively, it is clear that C_p is far too low. Currently we do not have a rigorous explanation for this. We hypothesize that the reverse velocity in the recirculation region is overprediced due to unaccounted viscosity effects or due to the discrepancy between the experimental and theoretical end conditions. An overprediction of the negative velocity can give rise to too small C_p values as is evident from the analysis in §4. However, the pressure recovery curve in Figure 9 does show the characteristic peak. Further, the peak appears near $St_H = 0.15$ as in the experiment.

Numerical solutions display broad-band frequency spectra, characteristic of shear layers. Characteristic flow patterns change with different forcing Strouhal numbers. Typical vortex structures for three flow regimes are depicted in Figure 10. The first, Figure 10(a), shows irregular agglomerations of vortex elements that appear in the absence of forcing. At the optimal forcing, $St_H = 0.15$, shown in Figure 10b, we observe that the actuator organizes the flow into large, well-spaced clusters of vorticity. Well beyond the optimal forcing, $St_H = 0.35$, the sinusoidal blowing and suction still organizes the flow, but the structures are not as pronounced.

5.3 Diffuser performance analysis with control-volume model

Tab. 1 displays the experimental and forced pressure recovery coefficients from experiment and the control-volume model. The reference planes of the pressure recovery coefficients are shortly before and near the exit of the diverging diffuser section. In the control-volume model, the same inlet profile is used for natural and forced case since the profile is nearly uniform and hardly changes under forced conditions.

Forcing is seen to strongly enhance the C_p value but the performance remains significantly smaller the potential flow value, which is considered as the upper bound. Apparently, small actuation cannot gave rise to a nearly uniform exit profile required for nearly optimum performance.

The theoretical C_p value of experimental data slightly overpredicts the experimental data. Overprediction was to be expected due to the neglection of the v-velocity and w-component in the derivation. A non-uniform pressure distribution may also contribute to the error.

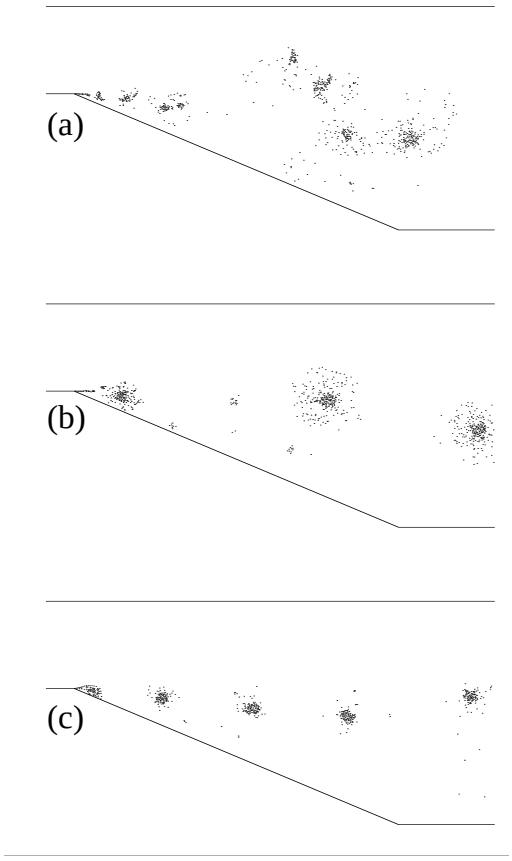

Figure 10: *Typical vortex structures for (a) unforced diffuser flow; (b) $St_H = 0.15$; (c) $St_H = 0.35$.*

Fluctuation is seen to reduce pressure recovery by 25% and 10% under natural and forced condition, respectively. Fluctuation hence seems to have an ambivalent role. On the one hand, it is a necessary prerequisite for mixing and a fuller exit profile, on the other hand it adds to the pressure losses. Note the absolute fluctuation penalty for forcing to the pressure recovery coefficient is very small, i.e. only 0.01 whereupon an benefit in terms of the C_p increase is 0.41. The true value for the pressure loss due to fluctuation is expected to be larger due to the neglected v-component. This neglected contribution may account for a large portion of the difference between experimental and model-based C_p values.

The control-volume model reveals that the pressure losses can mostly be attributed, analyzed and explained in the frame-work of momentum flux differences at the inlet and the exit — even under flow conditions with large-scale unsteadiness. Another intriguing conclusion is that the energy flux associated with turbulent kinetic energy hardly changes under forcing, the flux merely becomes more efficient in mixing high- and low-momentum fluid. This conclusion is consistent with corresponding observations in the experiment and modeling sections.

Table 1: *Control-volume model applied to the experimental data presented in Fig. 7. The superscript 'exp' refers to experimental data and 'cvm' refers to data from the control-volume model. The pressure-recovery coefficient is based on the maximum inlet velocity.*

case	unforced	forced at $30\,Hz$
H_2/H_1	2.64	
$\mathbf{C_p^{pot}}$	0.85	
$\mathbf{C_p^{cvm}}$	0.24	0.66
$\mathbf{C_p^{exp}}$	0.19	0.58
α_0^1	1.046	—
α_1^1	0.004	—
α_0^2	4.98	1.54
α_1^2	0.41	0.42
$C_p^{0,cvm}$	0.29	0.72
$C_p^{1,cvm}$	-0.05	-0.06

6 Discussion

A two-dimensional vortex model has successfully qualitatively (and to some extent quantitatively) reproduced the dominant features of a forced separated flow. This reduced-order model seems to capture the shear layer dynamics, the organizing effect of external (unsteady) forcing on the large-scale vortex dynamics and the wall effects surprisingly well. Consequently, performance enhancement (namely, the diffuser pressure recovery) due to unsteady forcing is also captured well by the model and validated by experiments.

However, there exist noticeable quantitative differences between the model and experiments. Examples are the over-predicted strength of the recirculation zone and the under-prediction of the pressure recovery. The discrepancies can partly be attributed to the assumption of two-dimensionality. Since the turbulent boundary layer may have or-

ganized three-dimensional structures and fine-scale turbulence (not resolved in the model), the extent mixing (of the high momentum free-stream flow with the near-wall flow) may be under-predicted; this will result in an under-prediction of the pressure recovery as well. Even two-dimensional direct Navier-Stokes simulations (at lower Re) at UTRC [18] displayed comparable discrepancies for similar reasons. Another simplification in the model is the inviscid flow assumption. This neglect of the no-slip condition and viscosity effect may be the reason for the over-predicted strength of the recirculation zone. Different end (particularly, inflow and outflow) conditions in the model (e.g. a straight channel extension following the expansion) and in the experiments (having a free exit for the expansion into the ambient) may also contribute to the discrepancies between the experiment and model.

7 Concluding remarks and outlook

We have demonstrated, using experiments in a planar diffuser and reduced-order models, that separation control can be achieved by exciting coherent vortical shear-layer structures. Exploratory experiments have shown that the pressure recovery of a highly separated diffuser flow can be significantly enhanced with low levels of external forcing. This suggests promise for obtaining large performance benefits with small control energy input. Under forced conditions, we show performance enhancement to be correlated with fuller exit mean velocity profiles and a pronounced vortex formation in a relatively narrow frequency band, corresponding to (non-dimensional) Strouhal frequencies between 0.1 and 0.2. These observations suggest that the unsteady forcing feeds energy into coherent vortex motion, thereby enhancing the exchange of momentum between the free-stream and near-wall flows. Similar experimental observations and interpretations have been noted by several investigators in the past (e.g. [7] studies of lift enhancement in flow past high-angle-of-attack airfoils). The lack of physics-based reduced-order models capturing such experimentally controlled flow features motivated our efforts to develop a moderate dimensional, vortex model for two-dimensional flow.

The hypothesis of exciting beneficial coherent structures for the pressure recovery is corroborated by our two-dimensional vortex model. The model establishes a reduced-order link between unsteady forcing and performance. The model simulation captures the spatiotemporal evolution of the large-scale shear layer dynamics in the separated flow region in that it describes the vortex roll-up, successive mergings and associated spreading, and broadband frequency spectra (validated by experimental measurements) reasonably well. In doing so, the model displays the sensitivity of the separated flow vortex dynamics to discrete frequency forcing (as observed in experiments). Most importantly, the pressure recovery improvement with an excitation of pronounced coherent vortex motion at a preferred frequency is correctly predicted. Optimal pressure recovery and preferred frequencies are in reasonable agreement with experimental measurements. The interpretation that forced mixing enhances the pressure recovery has been corroborated with control-volume analysis.

The present study is a part of ongoing efforts towards model-based flow control to guide prototype experiments, i.e. to predict natural and excitable flow phenomena, to suggest actuator distribution and to optimize control laws. Thus, expensive experimentation may be avoided by employing a hierarchy of physics-based models. Computationally inexpensive reduced-order models, similar to our 2D vortex model, enable exploratory studies for several control strategies while resolving only a few relevant flow phenomena. The control solutions suggested by these models may then be validated by high-fidelity simulations (typically, prohibitively expensive) such as large-eddy simulations. Novel control design based on application of control and optimization theory tools to the vortex models are currently being pursued and will be reported elsewhere.

Acknowledgements

This work was funded through UTRC Active Flow Control program (program manager Dr. Doug MacMartin) and Air Force Office for the Scientific Research Grant F49620-98-C-0006 (program monitor Dr. M. Jacobs). Authors acknowledge fruitful discussions with and comments by T.R. Bewley, F. Bertolotti, L. Cortelezzi, C.A. Jacobson, Y. Lifshitz, P. Lorber, D.C. McCormick, I. Mezic, R.M. Murray and R.W. Paterson.

References

[1] M. Gad-El-Hak and D. Bushnell. Status and outlook of flow separation control. In *29th AIAA Aerospace Sciences Meeting*, January 7-10, 1991 /Reno, Nevada, 1991. also as AIAA–91–0037 paper.

[2] H. Viets, M. Piatt, and M. Ball. Forced vortices near a wall. In *19th AIAA Aerospace Sciences Meeting*, AIAA–81–0256, St. Louis, MO, 1981.

[3] Jr. McKinzie, D.J. Delay of turbulent boundary layer detachmment by mechanical excitation: application to rearward-facing ramp. Technical report, NASA, 1996. Technical Report 3541.

[4] K. McManus and J. Magill. Separation control in incompressible and compressible flows using pulsed jets. In *27th AIAA Fluid Dynamics Conference*, AIAA–96–1948, New Orleans, LA, 1996.

[5] G. Hernandez, T. Schonfeld, F. Nicoud, and N. Mangiavacchi. Numerical active control of two-dimensional boundary layer separation. In *AIAA–96–2142*. 1st AIAA Theoretical Fluid Mechanics Meeting, June 17–20 /New Orleans, LA, 1996.

[6] D. Driller. Numerische Experimente zur selektiven Beeinflussung einer ablösenden, turbulenten Grenzschicht (transl.: Numerical experiments for a selective manipulation of a separating turbulent boundary layer, 1999. Diplom thesis, Fachbereich Mathematik, Technische Universität Berlin.

[7] I. Wygnanski and A. Seifert. The control of separation by periodic oscillations. In *18th AIAA Aerospace Ground Testing Conference*, June 20–23, 1994 / Colorado Springs, CO, 1994. also as AIAA–94–2608 paper.

[8] B. Nishri and I. Wygnanski. Effects of periodic excitation on turbulent flow separation from a flap. *AIAA Journal*, 36:547–556, 1998.

[9] L. Cortelezzi, A. Leonard, and J.C. Doyle. An example of active circulation control of the unsteady separated flow past a semi-infinite plate. *J. Fluid Mech.*, 260:127–154, 1994.

[10] L. Cortelezzi. Nonlinear feedback control of the wake past a plate with a suction point on the downstream wall. *J. Fluid Mech.*, 327:303–324, 1996.

[11] A.F. Ghoniem and K.K. Ng. Numerical study of the dynamics of a forced shear layer. *Physics of Fluids*, 30:706–721, 1987.

[12] R.V. Churchill and J.W. Brown. *Complex Variables and Applications*. McGraw-Hill, 1990.

[13] J.P. Giesing. Vorticity and Kutta condition. *J. Appl. Mech.*, 36:608–615, 1969.

[14] D. Shiels. *Simulation of Controlled Bluff Body Flow with a Viscous Vortex Method*. PhD thesis, California Institute of Technology, 1998.

[15] Robert D. Blevins. *Applied Fluid Dynamics Handbook*. Van Nostrand Reinhold Company, New York, 1984.

[16] S. Narayanan, B.R. Noack, A. Banaszuk, and A.I. Khibnik. Dynamic separation control in 2D diffuser. Technical Report 1.910.9901-4.1, United Technologies Research Center, East Hartford, CT, USA, 1999.

[17] D.C. McCormick. Boundary layer separation control with directed synthetic jets. In *39th AIAA Aerospace Sciences Meeting and Exhibit*, 1999.

[18] A.I. Khibnik, S. Narayanan, C.A. Jacobson, and K. Lust. Analysis of low dimensional dynamics of flow separation. In D. Henry and A. Bregeon, editors, *Proceedings of Ercoftac and Eurmoech Colloqium 383 — Continuation Methods in Fluid Dynamics, Aussois, France, September 6–9, 1998*, Notes on Numerical Fluid Mechanics **74**. Vieweg Verlag, 1999.

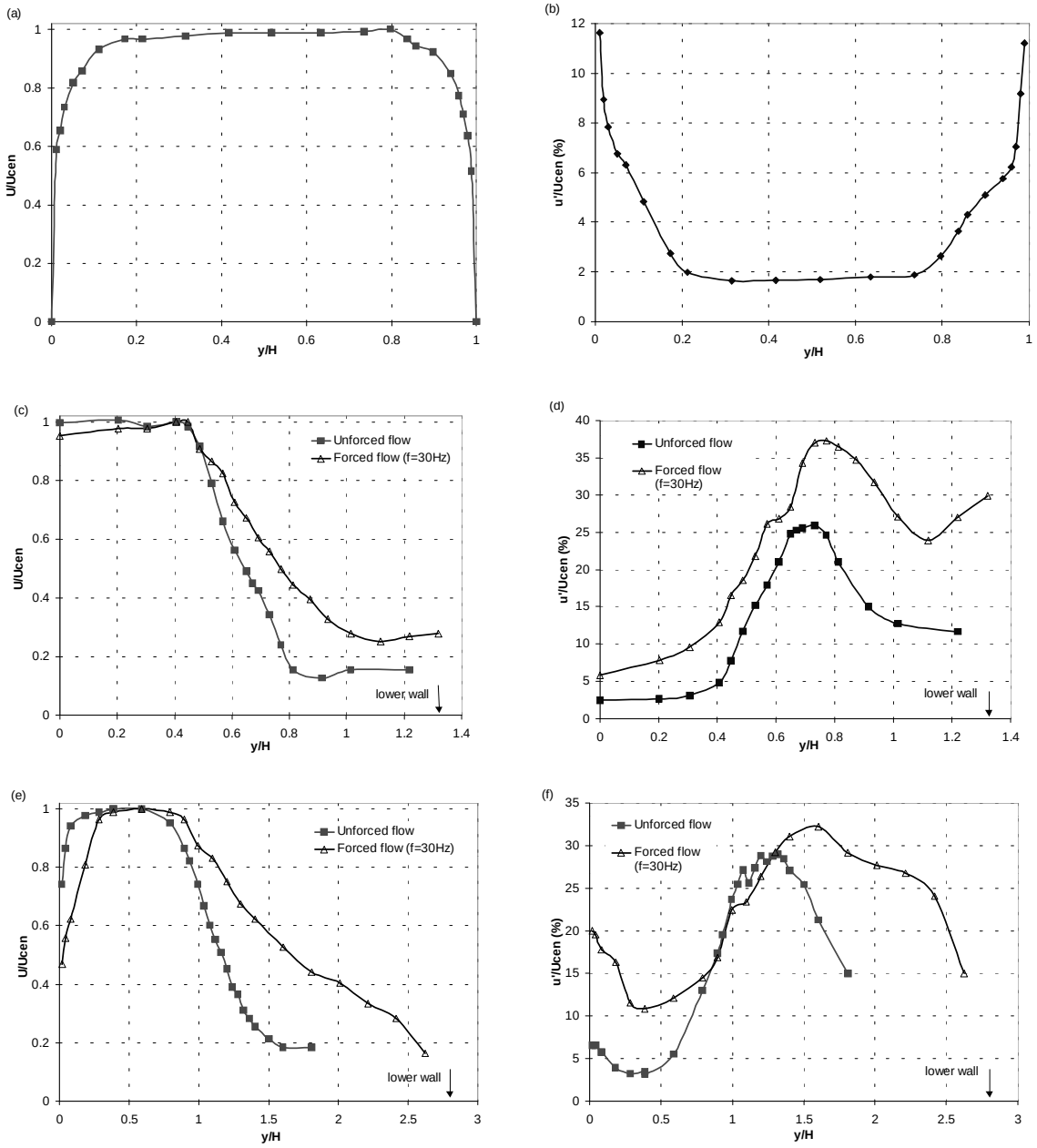

Figure 7: *Time averaged mean velocity (a,c,e) and rms-velocity (b,d,f) profiles at various streamwise locations in the diffuser for the unforced and forced flows. U_{cen} denotes the local centerline peak velocity, and H denotes the inlet channel height. For details see text.*